

Article

Mathematical and Physical Modelling of Transient Multi-Phase Flows in a Ladle Shroud during Start-Up

Daniel R. Gonzalez-Morales ¹, Bruno Girard ², Chantal Labrecque ², Mihaiela M. Isac ^{1,*}
and Roderick I. L. Guthrie ¹

¹ McGill Metals Processing Centre, McGill University, 3610 University Street, Wong Bldg. Room 2M040, Montreal, QC H3A 0C5, Canada; daniel.gonzalezmorales@mail.mcgill.ca (D.R.G.-M.); roderick.guthrie@mcgill.ca (R.I.L.G.)

² Rio Tinto Fer et Titane, 1625 Route Marie-Victorin, Sorel-Tracy, QC J3R 1M6, Canada; bruno.girard@riotinto.com (B.G.); chantal.labrecque@riotinto.com (C.L.)

* Correspondence: mihaiela.isac@mcgill.ca

Abstract: The Ladle Shroud has become an important part of secondary steelmaking, with its role in reducing liquid steel contamination and process improvements. Due to the inherent negative pressure at the lower nozzle–Ladle Shroud joint, it is well known that Ladle Shrouds, protecting steel flows between a Ladle and a tundish below, can suffer from inadvertent ingress of air. Therefore, there is a need to apply inert gas injection at the joint. In the present paper, 3D transient multi-phase simulations of flows occurring for a Reverse Tapered Ladle Shroud during start-up were studied using CFD software ANSYS Fluent 19.1. This allowed us to study the initial multi-phase flow developed during the start-up and potential steel reoxidation, based on a first principles approach. Time-dependent phase fields as well as attendant velocity and turbulence fields were obtained, resulting in the prediction of a turbulent multi-phase flow during start-up and filling. Additionally, some transient phenomena like steel splashing and air suction were observed mathematically. A full-scale water model of the Ladle Shroud was used to qualitatively validate the initial multi-phase turbulent flow inside the Ladle Shroud, in the absence of inert gas injection.

Keywords: Ladle Shroud; multi-phase flow; CFD modelling



Citation: Gonzalez-Morales, D.R.; Girard, B.; Labrecque, C.; Isac, M.M.; Guthrie, R.I.L. Mathematical and Physical Modelling of Transient Multi-Phase Flows in a Ladle Shroud during Start-Up. *Processes* **2023**, *11*, 1628. <https://doi.org/10.3390/pr11061628>

Academic Editor: Udo Fritsching

Received: 30 April 2023

Revised: 19 May 2023

Accepted: 23 May 2023

Published: 26 May 2023



Copyright: © 2023 by the authors. Licensee MDPI, Basel, Switzerland. This article is an open access article distributed under the terms and conditions of the Creative Commons Attribution (CC BY) license (<https://creativecommons.org/licenses/by/4.0/>).

1. Introduction

The Ladle Shroud is an essential device in modern steelmaking, separating the molten steel from the ambient atmosphere and thereby attempting to protect steel from being re-oxidized during its transfer from the ladle into the tundish. The connection between the ladle’s slide-gate nozzle, or “lower nozzle”, and the Ladle Shroud involves an overlap between the two parts. This overlap usually involves a gasket seal, as per Figure 1, through which argon is injected to displace any air. The final purpose is to avoid air suction and consequent liquid steel re-oxidation. However, it is known that air suction is a possibility, since the gauge pressure field generated within the Ladle Shroud can be expected to be negative at the lower nozzle–Ladle Shroud joint. This was noted in the early work of Wang, Lee, and Hayes [1], for example, where a negative gauge pressure (less than 1 atm) was demonstrated for a scaled water model of such a system. To avoid consequential air inhalation, argon shrouding has been adopted industrially in the hope of blocking air ingress. It has been found that depending on the ratio between the injected argon and the liquid steel flow rate, this will produce different multi-phase flow regimes within the Ladle Shroud itself. For instance, an argon shrouding flow at one-third that of the steel flow rate was found to be necessary to avoid air ingress, experimentally [2,3]. However, if the argon flow is too high, it will produce a large Tundish Open Eye (TOE) and subsequent slag entrainment, plus re-oxidation of liquid steel within the tundish. Quantitative research studies regarding these phenomena are still pending. In future, a more comprehensive

study is required to address the effect of the argon flow rates and Ladle Shroud designs on liquid steel cleanliness.

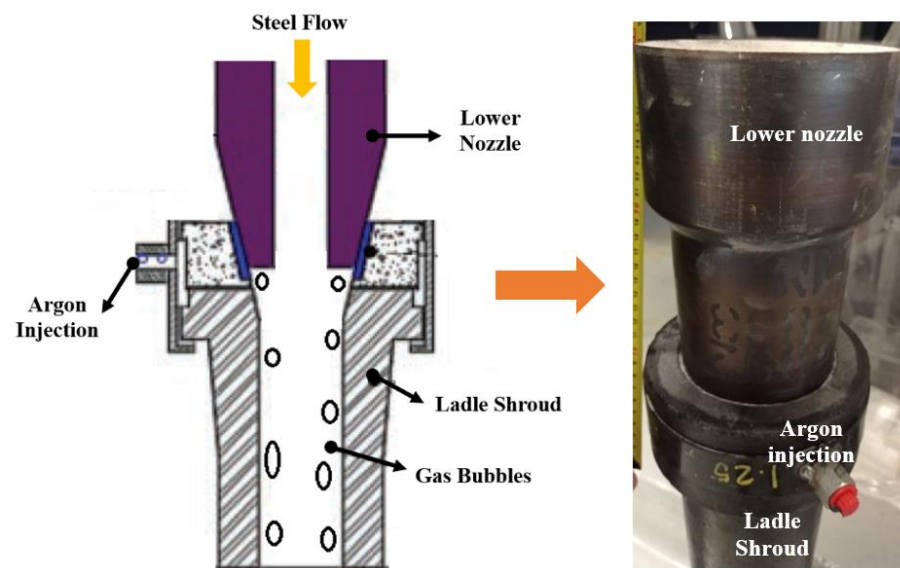


Figure 1. Schematic of the ladle–Ladle Shroud connection and the lower nozzle–Ladle Shroud joint.

Various studies have explored some improvements in the new Ladle Shroud process, such as new designs and argon injection techniques, using mathematical and physical modelling. For example, several new Ladle Shroud designs have been proposed over the last decade [4] aside from the traditional straight tube design. Two examples of these innovative designs are the Dissipative and the Trumpet (or reverse taper) Ladle Shrouds. It has been found that a dissipative design will enhance the intermixing phenomena within the Ladle Shroud–tundish system [5,6], and a trumpet design will reduce the entering velocity and turbulence of the steel into the tundish, to reduce slag entrainment and steel splashing [6,7]. Figure 2 depicts these two shroud designs. The use of a trumpet or reverse taper Ladle Shroud has become more common in the steelmaking industry, owing to the advantages it provides over the traditional straight, constant-diameter design during ladle changes. Studies of different Ladle Shroud designs have mainly focused on the steady-state regime via physical [2] and mathematical models [3,6,7]. Only a few transient studies have been performed thus far [7–9], focusing on start-up and ladle change operations and their impact on fluid flows and steel quality.

Mathematical modeling of Ladle Shroud–tundish systems has resulted in improved practices over the last few years. In 2018, Singh and Mazumdar [2] published a comprehensive water modelling analysis of two-phase Ladle Shroud systems and the effect of several variables, e.g., nozzle and shroud diameters, shroud gas flow, and particularly the gas to liquid flow ratio (Q_g/Q_l), on the flow characteristics within the Ladle Shroud. Two full-scale water models (for bloom and slab casting) were used for the experiments. The flow rate for the steel–water flow was equal, and for the air–argon flow, the rate was equal to the specified argon flow at 1873 K and 1 atm, with the slide gate fully opened in all experiments. Depending on the gas to liquid flow ratio (Q_g/Q_l), three general flow regimes were observed experimentally by Singh and Mazumdar [2]. For $Q_g/Q_l = 0.02$, a bubbly flow regime between the gas and the liquid was developed; for $Q_g/Q_l = 0.3$, two distinctive regions were generated: a free liquid jet in the upper Ladle Shroud part and a bubbly mixing zone in the lower part. Finally, with $Q_g/Q_l = 0.42$, the free jet extended completely within the Ladle Shroud, and a turbulent mixing zone initiated at the entrance to the tundish. Additionally, the authors simulated potential air ingress on the collector nozzle–shroud wall connection by connecting two of the three valves to manometers at ambient pressure under the different operating conditions and measuring the manometer arm differences ($+\Delta h$: air ingress; $-\Delta h$: air egress). For the different simulated gas to

liquid flow ratios, it was found that air ingress can be avoided provided that $Q_g/Q_l > 0.30$ for a submerged Ladle Shroud and $Q_g/Q_l > 0.42$ for a non-submerged Ladle Shroud. As such, the need to effectively shroud the ladle incoming steel flow with a sufficient inert gas flow rate was confirmed, and a threshold ratio was determined experimentally.

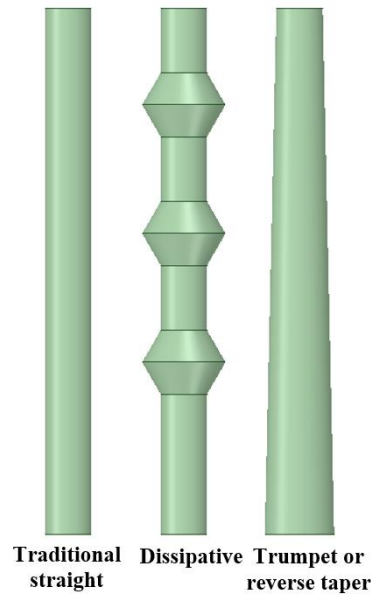


Figure 2. Different Ladle Shroud designs.

In 2019, Singh and Mazumdar [3] used the VOF multi-phase model to predict the steel–argon flow within the Ladle Shroud and compare this with previously published experimental results [2]. The model was validated extensively with experimental measurements, and the authors were able to present a correlation to predict the free jet length and the required gas flow rate to prevent air ingress. To model the turbulence flow field, the realizable $k-\epsilon$ model was used, and the surface tension force (F_σ) was added into the momentum equation as an extra term. The mathematical model results were compared with the water modelling experiments, where two regimes were observed. With a low gas to liquid flow ($Q_g/Q_l = 0.025$), a bubbly regime was observed, whereas when a higher gas to liquid flow ($Q_g/Q_l = 0.2$) was applied, a free steel jet regime was achieved. A gas liquid flow ratio of around $Q_g/Q_l = 0.4$ was needed to prevent any air ingress, where a full free jet was achieved within the Ladle Shroud [2].

Some more recent work on physical and mathematical modelling by Mukherjee and Mazumdar [10–12] validated the use of full-scale water models to study Ladle Shroud systems, given that the Reynolds number similarity is maintained and the isothermal approach was validated [10]. The authors also found that homogenous argon shrouding distribution was not achieved by the studied argon delivery systems [11]. Additionally, a new delivery system, which delivered the argon tangentially, was proposed, resulting in enhanced shielding of the lower nozzle–Ladle Shroud joint [11]. As well, the same authors further proved the usefulness of a water physical model, given the dynamic similarities, by studying the generated Tundish Open Eye (TOE) with different ratios of Q_g/Q_l , finding a linear relationship with the TOE area and the argon flow rate (Q_g) [12]. An empirical correlation was obtained to predict the area of the TOE based on operational parameters such as the liquid (Q_l) and gas (Q_g) flow rates.

The objective of the present work was to use the VOF multi-phase model to simulate the start-up operation for steel production in an industrial set-up and to analyze the attendant multi-phase flow phenomena when using an industrial trumpet/diverging Ladle Shroud. For this shroud, there was a 20 mm increase, from an initial top diameter of 50 mm to an exit diameter of 70 mm. The potential air suction for a 1.2 mm gap between the lower nozzle and Ladle Shroud was simulated. As well, a full-scale water model was constructed,

replicating as accurately as possible industrial system connections and details. The full-scale water model allowed us to experimentally observe the multi-phase flow behavior within the Ladle Shroud to validate the present simulations. The present work is helpful in determining the reasons for air infiltration, which will lead to a better understanding of the Ladle Shroud–tundish system dynamics in an effort to improve the behavior of these metal transfer operations and thus ensure improved metal cleanliness.

2. Materials and Methods

2.1. Mathematical Modelling

A mathematical model was developed, in which the actual geometry of the tundish entry zone was considered, referred to herein as “real case”, including the turnflow walls and the slide gate–lower nozzle parts. A transient, isothermal model was studied. Figure 3 presents the geometry, dimensions, and boundary conditions for the real case. All the boundary condition input values (namely steel and argon inlet mass flows) were taken from industrial operating conditions, provided by the steel plant, and adjusted to velocity values for the simulations.

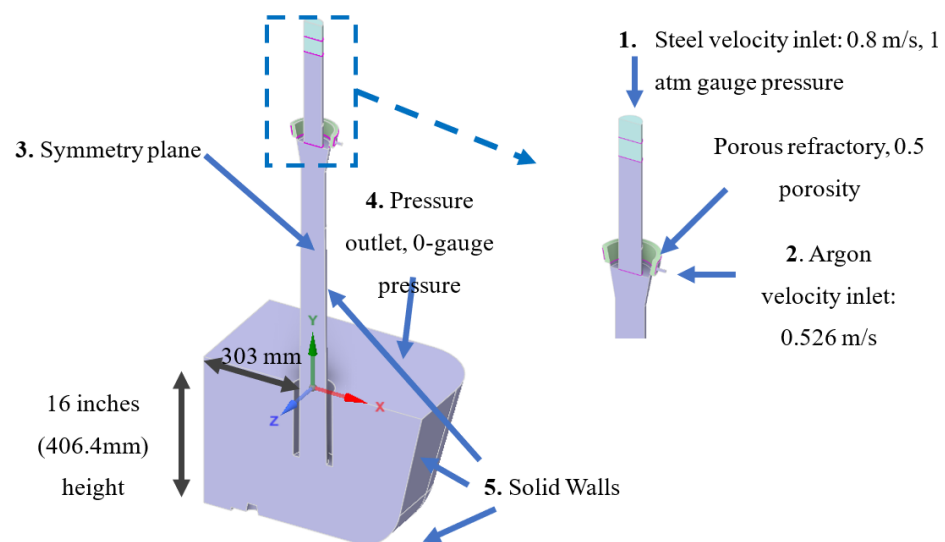


Figure 3. Geometry and Boundary Conditions for Real case.

A second case, allowing for air suction to occur, was also developed, to simulate and quantify the amounts of air inhalation to be expected. Figure 4 presents the geometry and boundary conditions for the air suction case. The same Ladle Shroud dimensions as for the real case were used, but the tundish zone was simplified to focus on air suction phenomena. Again, only half of the domain was considered, similar to the previous case.

Table 1 presents the properties of the three phases used in this isothermal model. The density and viscosity of the gas phases (air and argon) were referenced to 1873 K, based on the work by Singh and Mazumdar [3].

Table 1. Material properties at 1873 K.

	Steel (Liquid)	Air (Gas)	Argon (Gas)
Density, ρ (kg/m^3)	7000	0.5	0.3
Kinematic viscosity, μ (Pa s)	0.0056	1.78×10^{-5}	2.12×10^{-5}
Surface tension, σ (N/m)	-	1.7	1.6

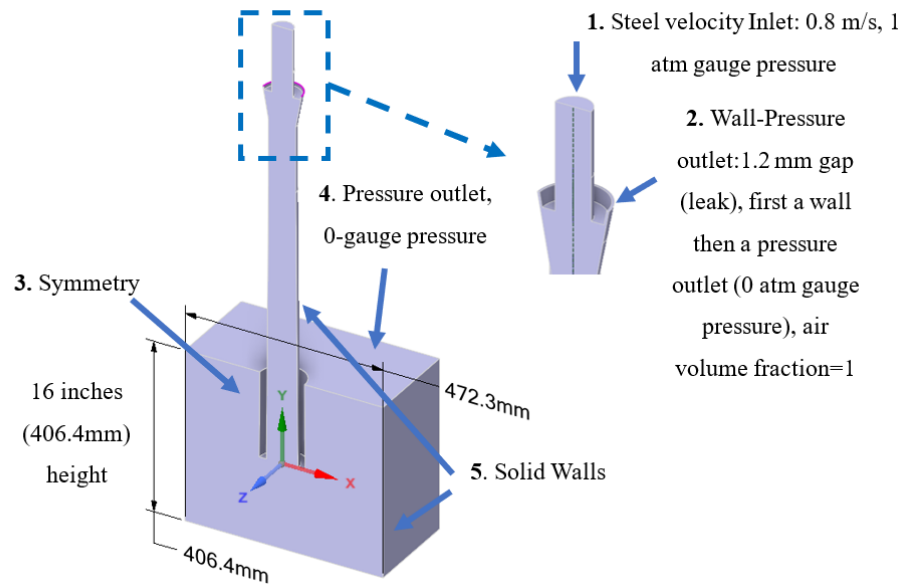


Figure 4. Geometry and Boundary Conditions for air-suction case.

The commercial CFD ANSYS Fluent 19.1 © was used to solve the flow field based on the solution of the required governing equations, which incorporated the Finite Volume Method (FVM). The selection of the multi-phase model, interface interactions, and turbulence model were done based on a literature review of the mathematical modelling of the Ladle Shroud system over the last five years. The equations requiring solution at each time step are presented below:

Volume of Fluid (VOF) multi-phase model continuity equation:

$$\frac{1}{\rho_q} \left[\frac{\partial}{\partial t} (\alpha_q \rho_q) + \nabla \cdot (\alpha_q \rho_q \vec{v}_q) \right] = \sum_{p=1}^n (\dot{m}_{pq} - \dot{m}_{qp}) \quad (1)$$

$$\sum_{q=1}^n \alpha_q = 1 \quad (2)$$

where ρ , α , and \vec{v} correspond to the density, phase volume fraction, and velocity, respectively, for the q th phase (steel, air, or argon), t corresponds to the time, and \dot{m}_{pq} and \dot{m}_{qp} correspond to the mass transfer from phase p to phase q and from phase q to phase p , respectively. Equation (2) indicates a constraint, where the sum of all the phase volume fractions must always equal unity. In this way, the volume fraction of the phases can be calculated via this constraint.

VOF explicit formulation discretization equation:

$$\frac{\alpha_q^{n+1} \rho_q^{n+1} - \alpha_q^n \rho_q^n}{\Delta t} V + \sum_f (\rho_q U_f^n \alpha_{q,f}^n) = \left[\sum_{p=1}^n (\dot{m}_{pq} - \dot{m}_{qp}) \right] V \quad (3)$$

Equation (3) corresponds to the discretization of the volume fraction via the explicit formulation equation in a time-dependent manner, where n , $\alpha_{q,f}^n$, V , and U_f^n correspond to the index of a previous time step, the face value of the q th phase volume fraction, the volume of the cell, and the normal volume flux through the face, respectively.

The momentum transport equation:

$$\rho \frac{\partial \vec{v}}{\partial t} + \rho (\vec{v} \cdot \nabla) \vec{v} = -\nabla p + \mu_{eff} \cdot \nabla^2 \vec{v} + \rho \vec{g} \quad (4)$$

$$\rho = \sum \alpha_q \rho_q \quad (5)$$

$$\mu_{eff} = \mu_t + \sum \alpha_q \mu_q \quad (6)$$

Equation (4) corresponds to a single momentum equation, which is solved and shared for all the phases. Equation (4) depends on the volume fractions of the phases via ρ and μ_{eff} , which are calculated via Equations (5) and (6) to obtain the volume fraction averaged density and effective viscosity, which includes μ_t , the turbulent viscosity calculated by the turbulence model. \vec{v} , p , and \vec{g} correspond to the mixture velocity, pressure, and gravity, respectively.

The standard k - ε turbulence model:

$$\mu_t = C_\mu \rho \frac{k^2}{\varepsilon} \quad (7)$$

$$\frac{\partial(\rho k)}{\partial t} + \nabla \cdot (\rho \vec{v} k) = \nabla \cdot \left[\left(\mu + \frac{\mu_t}{\sigma_k} \right) \nabla k \right] + G_k - \rho \varepsilon \quad (8)$$

$$\frac{\partial(\rho \varepsilon)}{\partial t} + \nabla \cdot (\rho \vec{v} \varepsilon) = \nabla \cdot \left[\left(\mu + \frac{\mu_t}{\sigma_\varepsilon} \right) \nabla \varepsilon \right] + C_1 \frac{\varepsilon}{k} G_k - C_2 \frac{\varepsilon^2}{k} \quad (9)$$

Equation (7) corresponds to the definition of the turbulent viscosity, where C_μ is a model constant (0.09), k corresponds to the turbulence kinetic energy, and ε corresponds to the dissipation rate. The terms are solved via Equations (8) and (9). G_k corresponds to the generation of turbulence kinetic energy due to shear work, and σ_k , σ_ε , C_1 , and C_2 correspond to model constants with values of 1.0, 1.3, 1.43, and 1.92, respectively.

Porous media equations:

$$\frac{1}{\rho_q} \left[\frac{\partial}{\partial t} (\gamma \alpha_q \rho_q) + \nabla \cdot (\gamma \alpha_q \rho_q \vec{v}_q) \right] = \gamma \sum_{p=1}^n (\dot{m}_{pq} - \dot{m}_{qp}) \quad (10)$$

$$\gamma \rho \frac{\partial \vec{v}}{\partial t} + \gamma \rho (\vec{v} \cdot \nabla) \vec{v} = -\gamma \nabla p + \gamma \mu_{eff} \cdot \nabla^2 \vec{v} + \gamma \rho \vec{g} - \left(\frac{\gamma^2 \mu_{eff}}{K} \vec{v} + \frac{\gamma^3 \mu_{eff}}{2} \rho |\vec{v}| \vec{v} \right) \quad (11)$$

where γ represents the refractory porosity. Equation (10) indicates the VOF continuity equation in the porous media, and Equation (11) represents the momentum transport equation in the porous media. The extra term on the right-hand side allows for the viscous and drag forces imposed by the porous walls onto the fluid.

Tetrahedral meshes with approximately 250,000 cells were generated, with a maximum skewness of 0.70. The simulations were run in the MMPC's High Performance computer, which comprises 5 nodes with 64 GB each and an Intel Xeon © processor. A maximum of 20 iterations were set for each variable timestep and adjusted to conserve a global Courant (Co) number of 0.25 using the explicit VOF formulation presented in Equation (3). The time steps ranged from 1×10^{-6} to 1×10^{-5} s. All the variables' residuals were set at 1×10^{-6} . The coupled algorithm velocity–pressure coupling [13] was used for the present simulations.

2.2. Physical Modelling

A physical modelling study of a specific Ladle Shroud–tundish system was performed using a full-scale water model [2,5,6,10–12]. This condition ensures that both Fr and Re dynamic similarities are conserved between water and liquid steel:

$$Fr_{model} \approx Fr_{full\ scale} \quad (12)$$

$$\frac{u_{model}}{\sqrt{gL}} = \frac{u_{full\ scale}}{\sqrt{gL}} \quad (13)$$

$$Re_{model} \approx Re_{full\ scale} \quad (14)$$

$$\frac{u_{model}L}{\nu_{water}} = \frac{u_{full\ scale}L}{\nu_{steel}} \quad (15)$$

where L corresponds to the characteristic longitudinal lengths of both the model and steel prototype Ladle Shrouds. The velocity u is also preserved between the two, since $\nu_{water} \approx \nu_{steel\ at\ 1873\ K}; 1 \times 10^{-6} \approx 0.916 \times 10^{-6} \text{ m}^2/\text{s}$. As such, the Fr and Re dimensionless numbers are virtually equivalent, allowing for an almost exact replication of the liquid metal flow phenomena within the two-phase Ladle Shroud–tundish systems. Given the transparency of water, and the safety and simplicity of performing room temperature experiments, this explains the value of water models in elucidating flow phenomena in steelmaking systems. Quoting recent examples, good correlations between experimental and mathematical results with full-scale water models in multi-phase analyses were obtained [2,5,6,10–12,14,15], in keeping with previous works, showing water–air modelling to be an accurate representation/approximation of the liquid steel–gas interactions and multi-phase flow behavior.

For the construction of the full-scale model, diagrams and real parts provided by the industrial partner were used to exactly replicate the dimensions and intricacies (mainly the lower nozzle–Ladle Shroud connection) of the Ladle Shroud–tundish system. It is important to mention that, to focus on the Ladle Shroud design’s transient performance, a complete water model did not have to be constructed, but only a sub-system addressing the entry flow of steel into the tundish. This was identical to the mathematical model for producing a digital twin. The resulting flow visualization will be presented for comparison with the mathematical modelling results now predicted.

Thus, Figure 5 presents a CAD visualization of the complete ladle–tundish system’s inner volume and a corresponding close-up of the detail of the part of study in the present work, the connection between the ladle and the tundish, namely the well block, an upper slide gate nozzle, the slide gate, the lower nozzle, the Ladle Shroud, and the truncated inlet section of the tundish. This CAD geometry was generated to ensure all the internal and necessary dimensions for the volume used for the mathematical model. These, in turn, were replicated in the water model of the system, as obtained from diagrams provided for the actual industrial system.

Figure 6 depicts the dimensions (diameters and heights) of the different parts to be built for the transparent plastic (PVC or Plexiglas) Ladle Shroud. The dimensions were respected as much as possible, with some minor adjustments being necessary during the construction and assembly of the parts. Figure 6 also shows an actual lower nozzle and Ladle Shroud made of a refractory material, with the overlapping connection and the argon injection location. The same figure reveals that the connection between the lower nozzle of the slide gate and Ladle Shroud is just an overlap between a male–female connection and an interspersed soft gasket. As no extra seal or protection is used, there is an absolute need for the injection of argon to oppose any ingress of air, as previously mentioned.

For the construction of the water model, only the parts below the slide gate, meaning the lower nozzle and Ladle Shroud, were built, as a previous full-scale ladle slide-gate water model set-up was already in place within the MMPC’s (McGill Metals Processing Center) water modeling laboratory, with very similar dimensions. A height adjustment to the lower nozzle, from 254 to 215 mm, was performed to compensate for the height of the parts already in place and respect the total height of 1580 mm between the bottom of the ladle and the bottom of the Ladle Shroud in the corresponding industrial set-up. That adjustment allowed us to maintain the full-scale Re and Fr numbers in dynamic similarity.

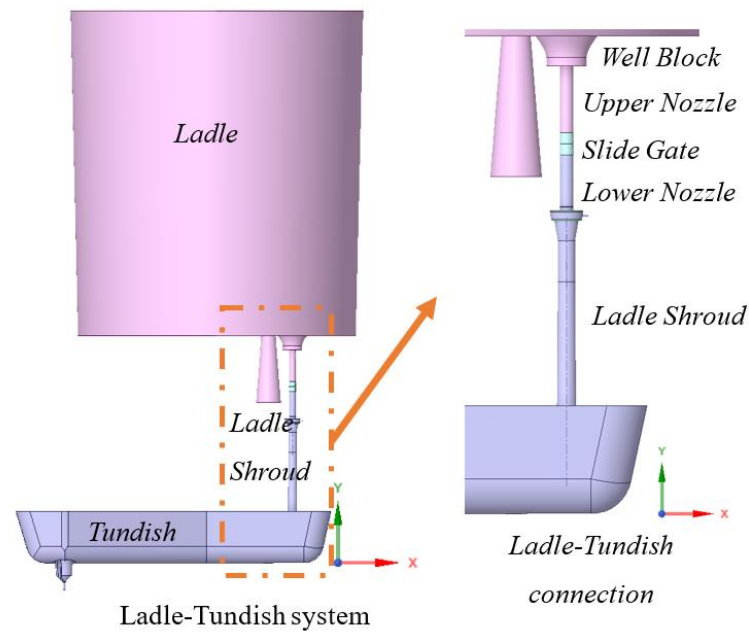


Figure 5. Diagram of the ladle–tundish system and close-up of the ladle–tundish connection.

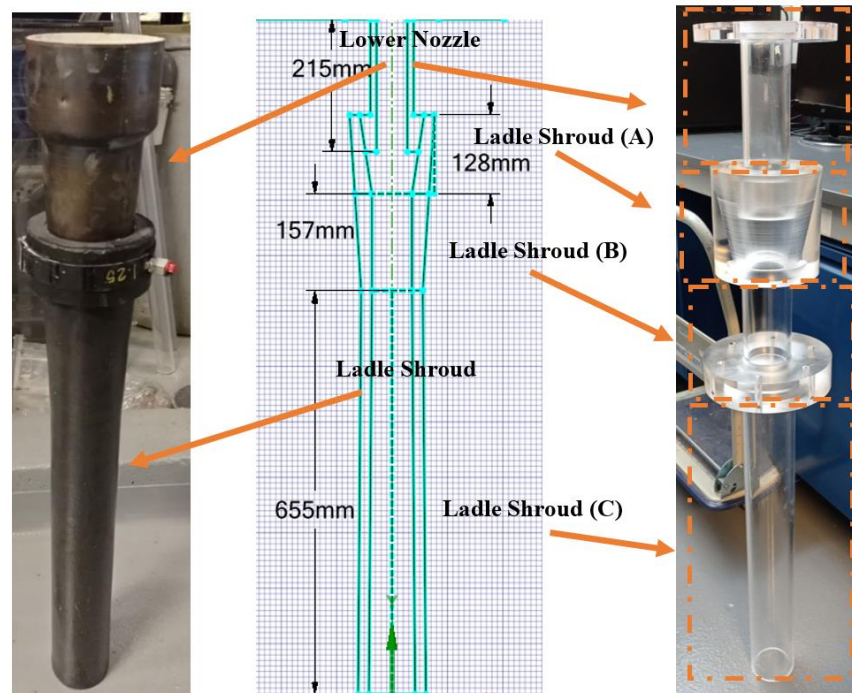


Figure 6. Actual Ladle Shroud, schematic, and final water model.

Similarly, the total height of the Ladle Shroud was set equal to that of the industrial set-up, i.e., 880 mm. In addition, to construct this transparent Ladle Shroud and respect the changes in different inner diameters in the real system, this was divided into three segments (A), (B), and (C), as presented in Figure 6.

The Ladle Shroud I part, according to the corresponding industrial set-up, presents a diverging ID from 65 to 75 mm over a 655 mm drop height. Due to the complexities and unavailability of a transparent plastic to be manufactured with said dimensions, it was decided to instead use a 70 mm ID (2-3/4 inches) with a 655 mm height transparent PVC pipe, with 70 mm being the average diameter of the real diverging Ladle Shroud. This adaptation is not considered to dramatically affect our sought similarity between the

industrial process and the water model. The three parts of the Ladle Shroud were glued together, and a connecting flange was used between part (B) and (C), to be subsequently attached to the slide gate.

For the construction of the tundish model for the water modelling research, it was decided to adapt and construct the first portion of the tundish, meaning the first 1041 mm in length. This is only for the present work, for which only steel flow phenomena in the Ladle Shroud and tundish entry zone were to be studied, as shown in Figure 6, below.

The physical model reproduces the first 1041 mm of the volume of the tundish, without the rounded edges, using 12.7 mm (1/2 inch) thick Plexiglas sheets. The tank presents the same height as the industrial tundish of 670 mm. An inner dam (which can be removed) was located 80 mm from the left-hand side wall to maintain a quiescent quasi-steady state flow at 406.4 mm (16 inches), being the operational steel level height. The inner dam acts to always maintain the maximum level of steel in the tundish. The overflow of water pours over the dam, and this output of water flows down to drain through a 76.2 mm (3 inch) hole, set at the bottom of the exit port. The Plexiglas 17 inch sheets were cut and assembled.

An aluminum support frame sat on an existing large tundish tank from a previous set-up in the MMPC water modelling laboratory. Before the experiments, water tests were carried out to determine the inlet flow, based on the existing slide gate aperture. The slide gate opening for a 0.8 m/s inlet velocity (1.6 L/s) was determined to be approximately equal to a quarter opening of the slide gate nozzle.

Video recordings of the filling stage of the system with water were made, to analyze and compare with the mathematical predictions: i.e., the multi-phase flow generated within the Ladle Shroud, steel-argon/air in the industrial set-up system, and water-air in the physical model. Figure 7 depicts the complete experimental set-up, where the slide gate, Ladle Shroud, and longitudinally truncated tundish tank can be observed, ready for water model experiments. The position of the Ladle Shroud was adjusted with respect to the tundish tank. One experimental case was performed 3 different times as a baseline, using the inlet water flow of 1.6 L/s without gas shrouding and with an airtight seal between the lower nozzle and Ladle Shroud parts. A video recording was taken, with a GoPro Hero 6 © video camera with a 1080p resolution and 40 frames per second, from several different views for subsequent analysis.



Figure 7. Experimental set-up with water model Ladle Shroud and tundish tank.

3. Results

Time-dependent phase volume fraction contours for the three phases were calculated for the real case and are presented on the symmetry plane in Figures 8–10, ranging over timeframes from 0.57 s to 77.8 s. At 0.574 s, the predicted steel volume fraction contour shows that, initially, the falling steel stream breaks into two streams when reaching the bottom part of the lower nozzle at the joint with the Ladle Shroud, where the ID changes from 50 to around 80 mm. The stream on the right-hand side breaks into steel droplets, owing to its rapid acceleration in free-fall, and consequent Helmholtz Instability, which were possibly enhanced by crossflow impingement of the transverse flow of argon. However, as this effect was not observed in the previous simulations, it can be assumed that surface tension forces introduced in the simulations were the main factor contributing to the prediction of the initially observed falling steel droplets. At 4 s, the falling steel stream stabilizes into one single stream, similar to the results predicted from previous cases. The stream then collides with the turnflow at the bottom, generating splashing. One can observe steel droplets ejected to considerable heights near the curved wall on the right-hand side of the tundish. The corresponding argon volume fraction contour, at the same time, shows that the argon shrouding effect is more distinct on the right-side injection point, whilst the argon barely reaches the opposite left side at 4 s. Figure 9 presents the predicted phase volume fraction contours at 13 and 30 s. The steel and air volume fraction contours predict that some air entrainment on the right-hand side near the turnflow walls will be produced due to the high incoming turbulence of the steel stream at 13 s. These gas bubbles will be consistent throughout the filling stage. The corresponding argon gas volume fraction contour, at the same time, predicts a more even and symmetrical gas distribution in the top part of the Ladle Shroud, reaching almost half of the Ladle Shroud height. At 30 s, when the steel level is about to reach the bottom of the Ladle Shroud, air bubbles can be observed within the liquid steel, practically all along the domain width, according to the steel and air contours. The maximum size of the air bubbles is around 20 mm in diameter. The corresponding predicted argon volume fraction contour shows an asymmetrical argon distribution down the Ladle Shroud, likely due to the complexity of the phase interactions and the need for the argon flow to overcome the steel surface tension force to maintain a constant flow along the Ladle Shroud. Additionally, a few argon bubbles can be observed on the symmetry plane; however, air predominates at the 30 s mark. The gas bubble composition largely corresponds to air at 30 s. Figure 10 shows the phase contours at 35 and 78 s, during the final stages of the filling process. At 35 s, the Ladle Shroud starts to fill inside with steel, thereby generating a highly multi-phase turbulent flow within it, as seen for the simplified case. The corresponding air volume fraction contour shows that air remains within the Ladle Shroud and is not yet eliminated after 78 s of steel flow. At that moment, the steel height reaches its steady-state operating level of 16 inches. Note that the predicted steel and argon contours depict gas bubbles within the Ladle Shroud, plus some bubbles within the liquid steel in the tundish. Some predicted sizes of the argon bubbles are similar to those observed from previous water model systems during steady-state operation (i.e., 4–8 mm bubbles). However, bigger-sized bubbles, with maximum diameters of approximately 20 mm, are also present within the Ladle Shroud. The argon shroud distribution in the top part of the Ladle Shroud then presents a stable and symmetrical distribution under quasi-steady state operation, presenting a partial liquid free jet regime, as defined by the work of Singh and Mazumdar [2,3]. Additionally, it is worth mentioning that at 78 s, the porous region is not filled completely with argon (top left part). This is presumably because the argon flow is insufficient to disperse air within the total porous region.

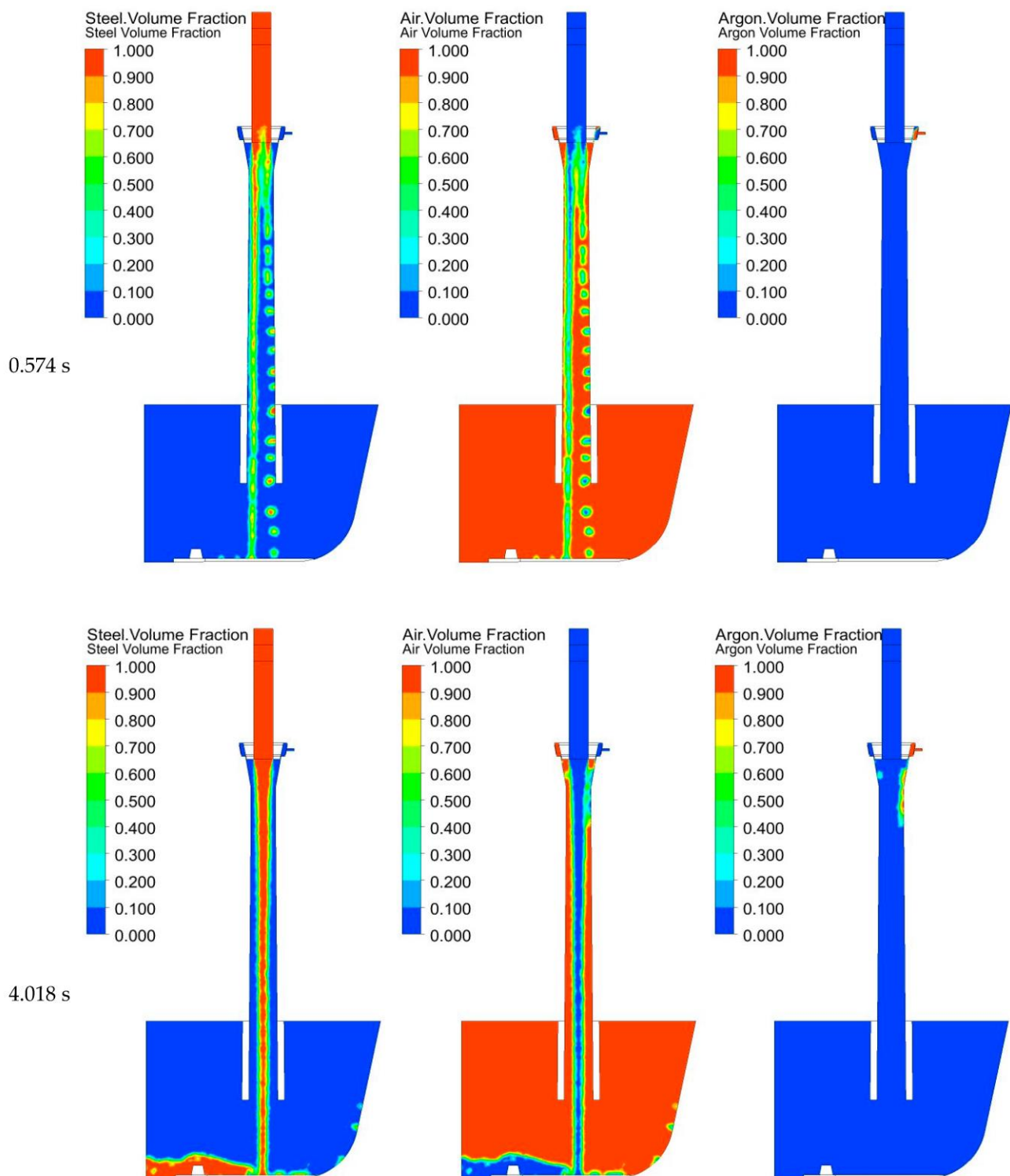


Figure 8. Predicted phase volume fraction contours for steel, air, and argon phases at 0.574 and 4.018 s on the symmetry plane.

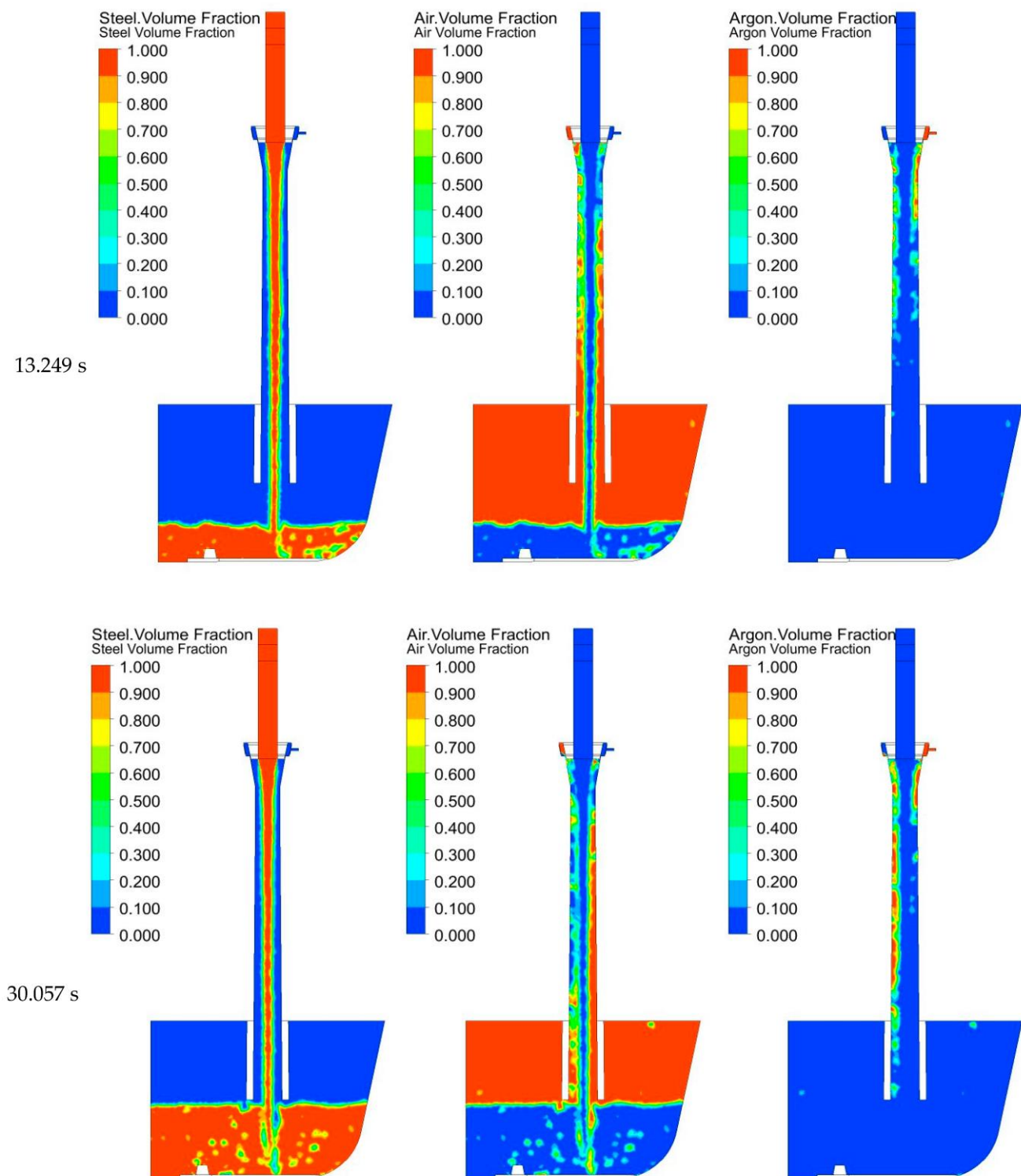


Figure 9. Predicted phase volume fraction contours for steel, air, and argon phases at 13.249 and 30.057 s on the symmetry plane.

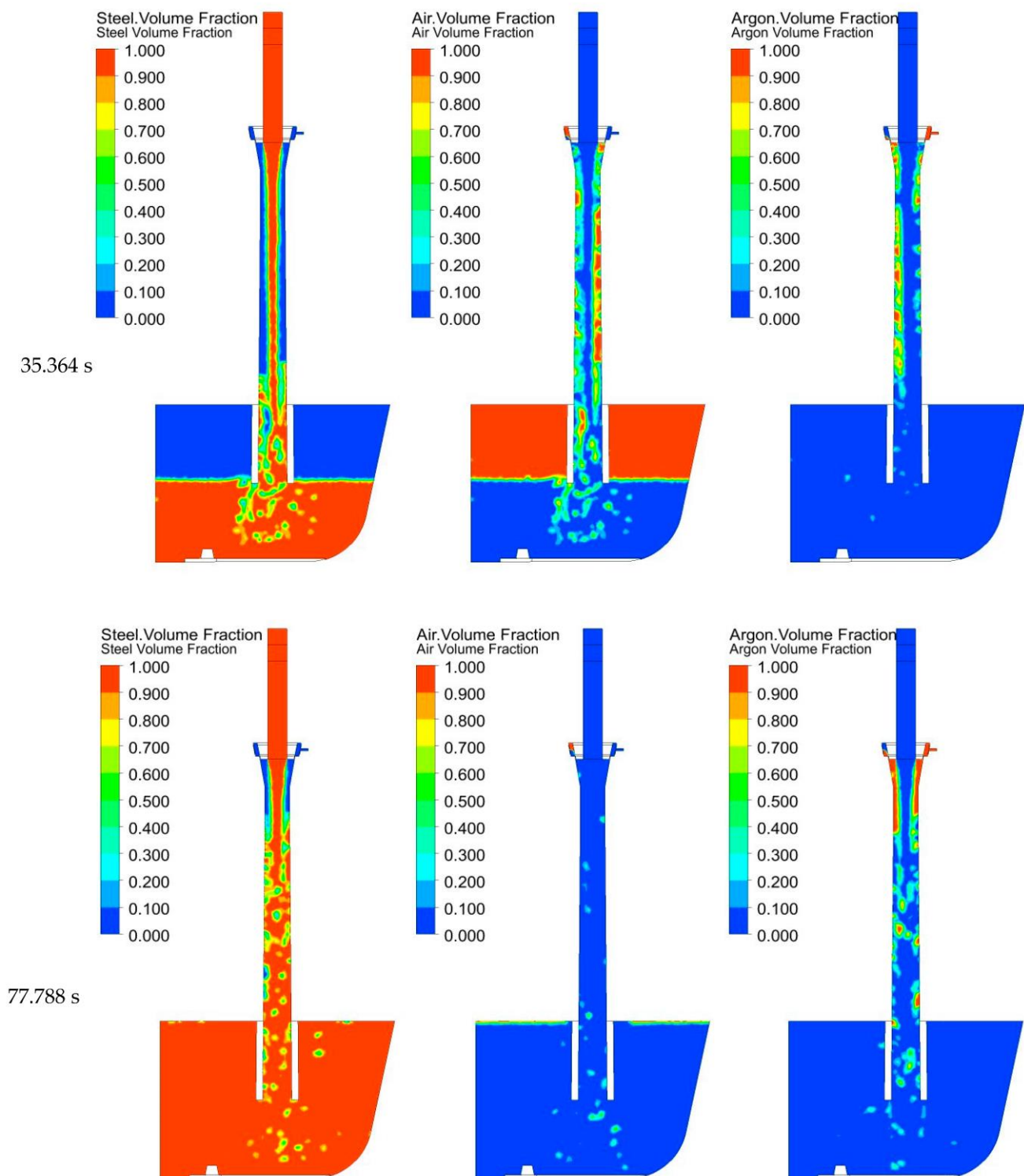


Figure 10. Predicted phase volume fraction contours for steel, air, and argon phases at 35.364 and 77.788 s on the symmetry plane.

To complement the previous results for the different phases on the symmetry plane, 3D visualizations of the simulation were generated via Volume Rendering, where the volume is split in 100 planes parallel to the symmetry plane to obtain an inner view of the filling stage at different time steps for the steel volume fraction only. Figures 11 and 12 present these results in an isometric view towards the inside of the system, from 0.6 to 80 s. At

0.6 s, the two diverging streams can be observed again, which then stabilize into a single stream at 3.3 s. At this moment, the splashing is readily evident and dramatic, with steel droplets reaching almost to the end of the calculation zone on the vertical +y axis. This can partly be attributed to the effect of the turnflow during the initial time steps, as its walls redirect the liquid steel into the back part of the entering zone, generating splashing mainly on the right-hand side. Afterwards, at 5 s, the splashing height diminishes, as the flow then becomes more quiescent at 7.2 s, where gas (air) bubbles start to become present within the liquid steel. At 17 s, the presence of gas bubbles is more evident, and at 32.5 s, gas bubbles extend widely throughout the liquid steel in the tundish entry zone, with some bubbles even reaching the back wall of the tundish. At the same time, the single falling steel stream “breaks”, generating turbulent intermixing of the phases inside the Ladle Shroud. Figure 12 presents the predicted 3D steel fraction volume rendering at 35 s, 40 s, and 80 s. As the steel level keeps rising within the Ladle Shroud, (around 8.5 inches in height at 35 s), the gas bubbles start to be confined near the exit zone and are less extended within the liquid steel, as the flow within the Ladle Shroud starts to present high intermixing between the three phases, confining the gas bubbles mainly within the Ladle Shroud. Then, at 40 s, this effect increases, as a highly turbulent flow is constrained to gradually fill the Ladle Shroud. By 80 s, when the steel level reaches 16 inches, a predominantly bubbly argon–liquid steel flow regime is predicted, with the presence of large argon bubbles along the Ladle Shroud, under quasi–steady state operations. The size of these argon bubbles is around 15 mm diameter. These, when exiting the Ladle Shroud, and rising to the liquid steel surface within the tundish, can be expected to disturb the overlaying 1.5-inch slag layer. This, in turn, can promote slag entrainment in the form of small inclusions, as demonstrated earlier experimentally and numerically [8,9,15].

A four-phase study, adding the slag phase to the simulation, is necessary to address the effect of the injection of argon on the size of the Tundish Open Eye (TOE) and potential slag entrainment, using a complete VOF multi-phase model rather than a DPM-VOF model combination [9], where the argon bubble size is pre-assumed and homogenous. The present results suggest this might be an important underestimation of the phenomena occurring within the Ladle Shroud.

Figure 13 shows the predicted velocity and turbulence kinetic energy contours at 80 s on the symmetry plane under quasi–steady state operation. The velocity field (see Figure 13a) predicts an important acceleration of the flow in the zone where the falling steel stream encounters the perpendicular argon injection. The stream then progressively slows until reaching an exit velocity from the Ladle Shroud at around 0.5 m/s. Therefore, the Ladle Shroud design fails to decelerate the steel flow markedly, which is the main purpose of the diverging ID Ladle Shroud design. The turbulence kinetic energy contour (see Figure 13b) shows a high turbulence zone at the top part of the Ladle Shroud (maximum values of $0.5 \text{ m}^2/\text{s}^2$) due to the interaction between the liquid steel and the argon injection. This will lead to wall shear stress values of around 15–30 Pa on the Ladle Shroud wall, according to Figure 14, generating higher wall shear stress on the Ladle Shroud walls than on the turnflow walls, where values of 3 to 6 Pa are predicted. Through the analysis of the results of the “real case”, the following results can be extracted:

- A highly turbulent multi-phase flow will be generated during the initial filling stage of the system, caused by the collision of the falling steel stream with the base and sidewalls of the turnflow.
- Steel stream “breakage” is observed when the steel level reaches the bottom part of the Ladle Shroud, promoting the generation of air bubbles (~20 mm), as observed in Figure 10, where at 35 s, gas bubbles are observed on the symmetry plane phase contour for air.
- The total volume of air bubbles within the liquid steel in the tundish decreases with time, meaning that at a higher level of steel in the tundish, the air fraction within the bubbles will gradually decrease within the steel (Figure 10, 78 s); then, bigger argon bubbles will be produced by the argon injection.

- The effective displacement of the initial air in the system, caused by flow of liquid steel and argon injection into the shroud, is a relatively slow process. It is 33 to 70 s in the present simulations; however, in practice, this can take longer, given only the entrance portion of the tundish was accounted for in the simulations, making the steel highly prone to reoxidation during that period.

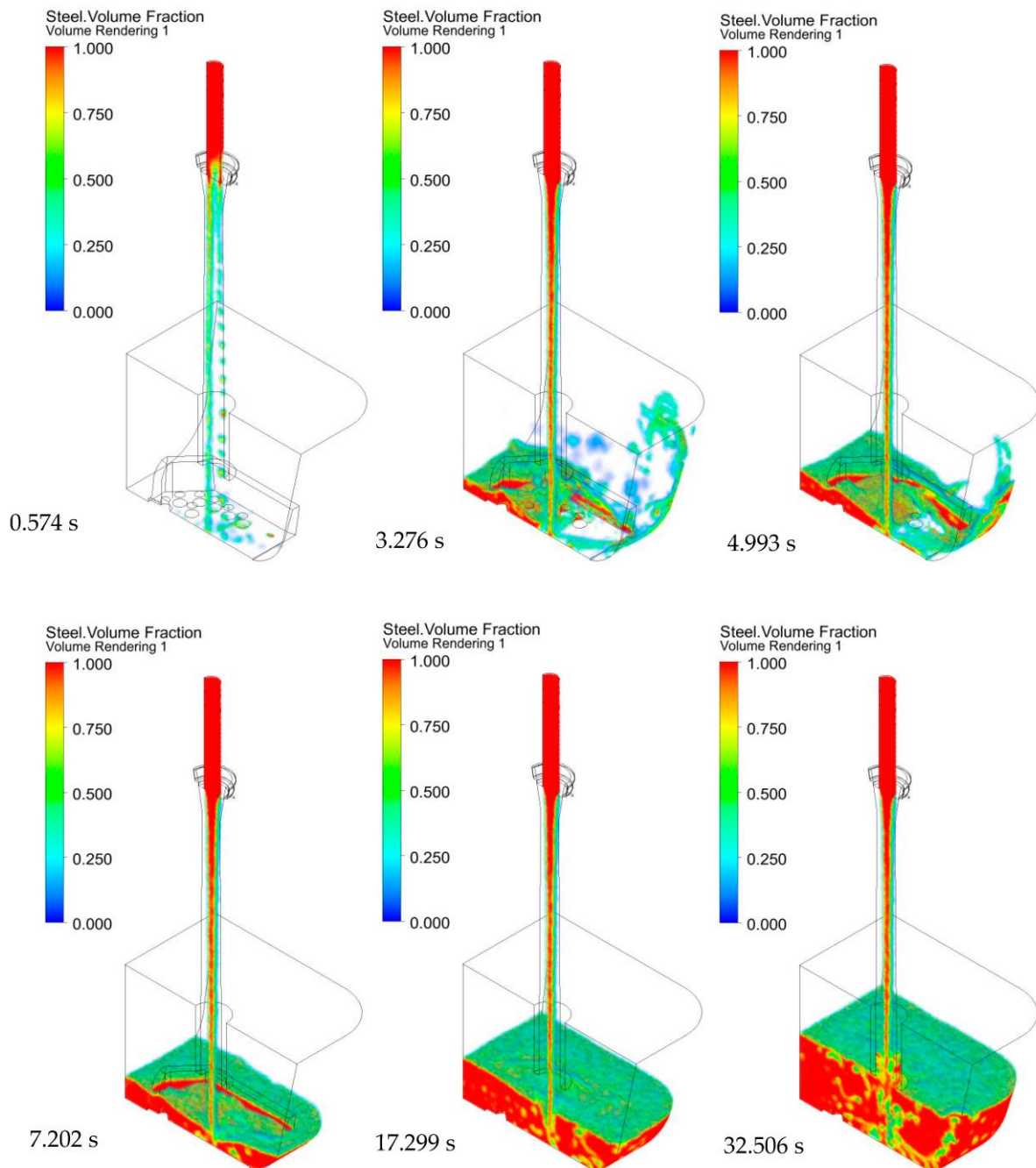


Figure 11. Predicted steel volume fraction 3D contours at different times in isometric view.

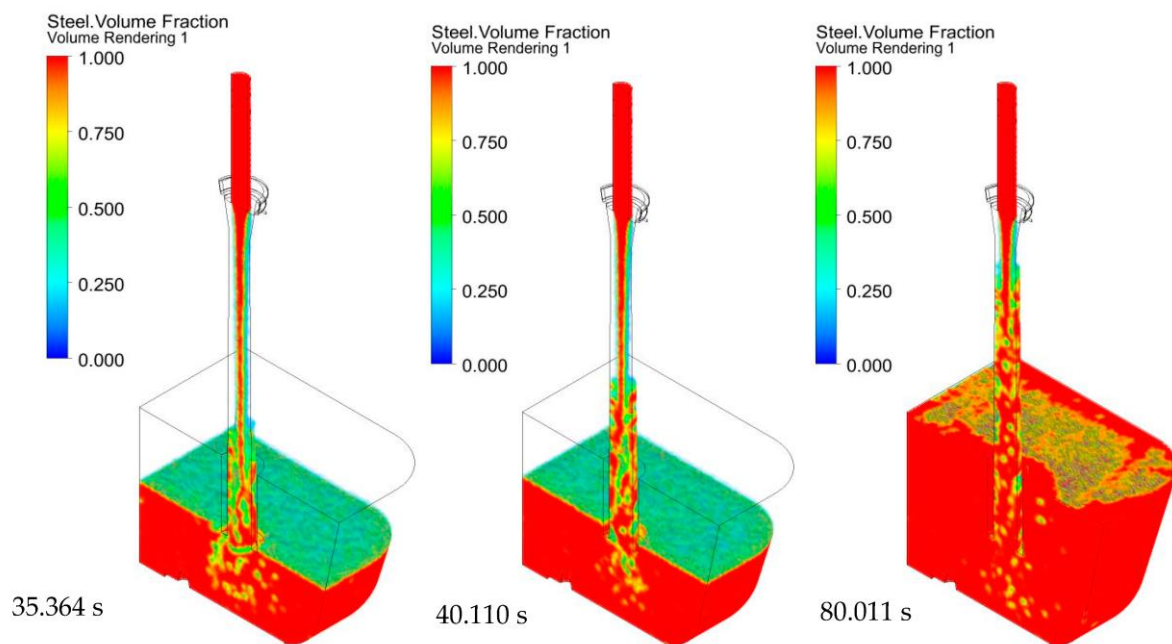


Figure 12. Predicted steel volume fraction 3D contours at different times in isometric view.

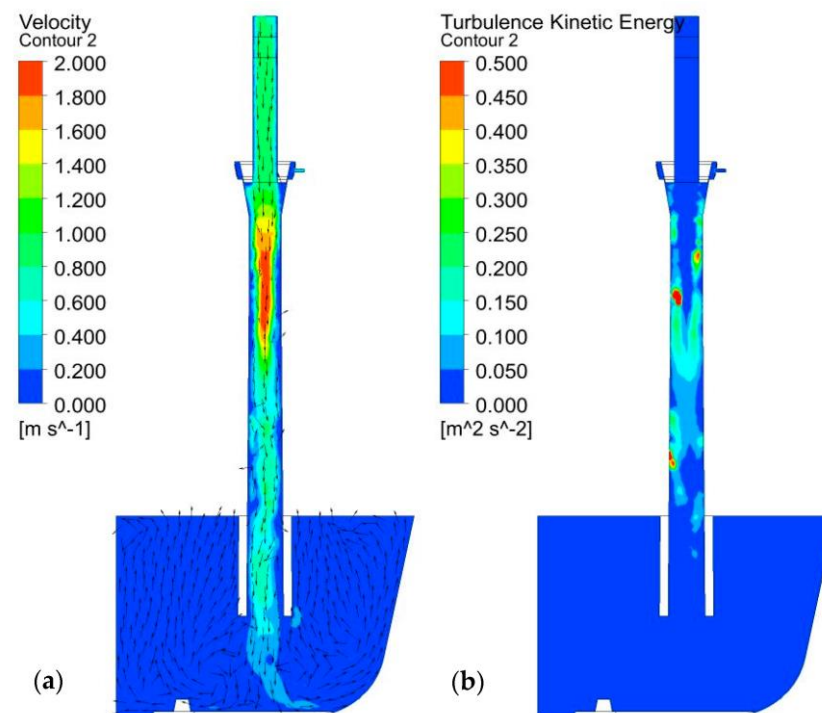


Figure 13. (a) Predicted velocity and (b) turbulence kinetic energy contours at 80.011 s on the symmetry plane.

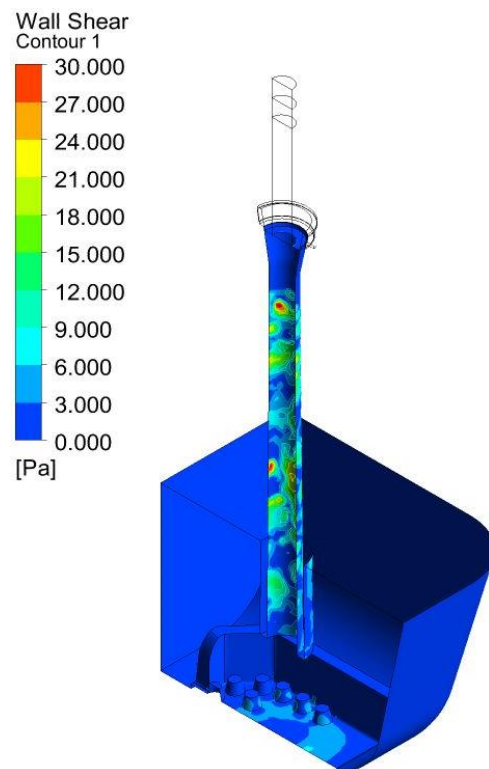


Figure 14. Predicted wall shear stress on the Ladle Shroud walls and tundish at 80.011 s in isometric view.

The process followed for the present air suction case is similar to the simulation performed for the real case. Therefore, the steel volume fraction contours during the filling stage are the same in practice, since the argon flow only slightly affects the velocity field. Figure 15a depicts the steel volume fraction contour at 41.8 s. At this point, the Ladle Shroud can be seen to be nearly filled with liquid steel, with some air bubbles present along the Ladle Shroud. The corresponding absolute pressure contour, as shown in Figure 15b, presents a negative pressure field at the top. The absolute pressure at the top portion ranges from 0.416 to 0.582 atm; the simulation was stopped at 41.853 s to change the boundary conditions and allow for in-leakage of air through a 1.2 mm gap between the slide gate nozzle and the Ladle Shroud. Figure 16 shows the predicted steel volume fraction and absolute pressure contours at 42.154 s, 0.3 s after the boundary condition was changed. This dramatic change can be seen in Figure 16a, where the steel volume fraction contour shows the zones near the Ladle Shroud walls with a steel volume fraction equal to 0 (blue color), meaning an air volume fraction equal to 1. This is confirmed in Figure 17, where the velocity contour is presented at 42.154 s, indicating zones with air velocities higher than 5.0 m/s near the Ladle Shroud walls. An instantaneous air flow of 314.75 L/min of air is predicted through the 1.2 mm gap surface. The absolute pressure contour changed (from Figure 15b to Figure 16b) 0.3 s after the boundary condition change. The predicted values within the Ladle Shroud changed to 1 atm absolute pressure along almost the whole of its height, as the system was “open” to atmospheric pressure (1 atm). The previous computations prove that the pressure difference between the Ladle Shroud and the atmosphere will generate an important air inflow into the system, unless a perfect seal between the mating parts (lower nozzle and Ladle Shroud) cannot be adequately accomplished. This will compromise the quality of the liquid steel, showing the risks of leaks in the system, which will lead to high re-oxidation and to a significant amount of alumina inclusions. The previous results additionally show and quantify, for the first time ever, the potential for air suction in Ladle Shrouds via mathematical modelling.

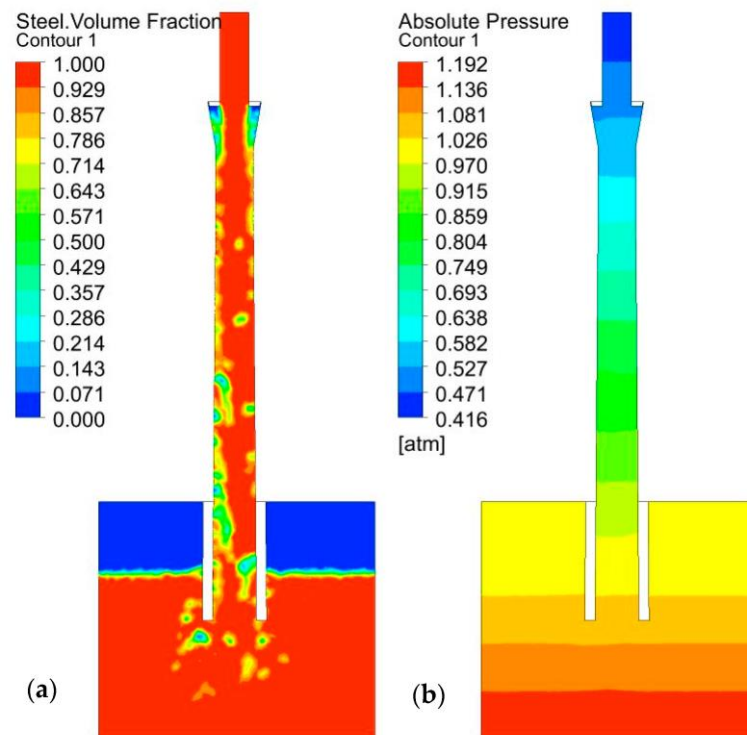


Figure 15. Predicted contours for (a) steel volume fraction and (b) absolute pressure at 41.853 s on the symmetry plane.

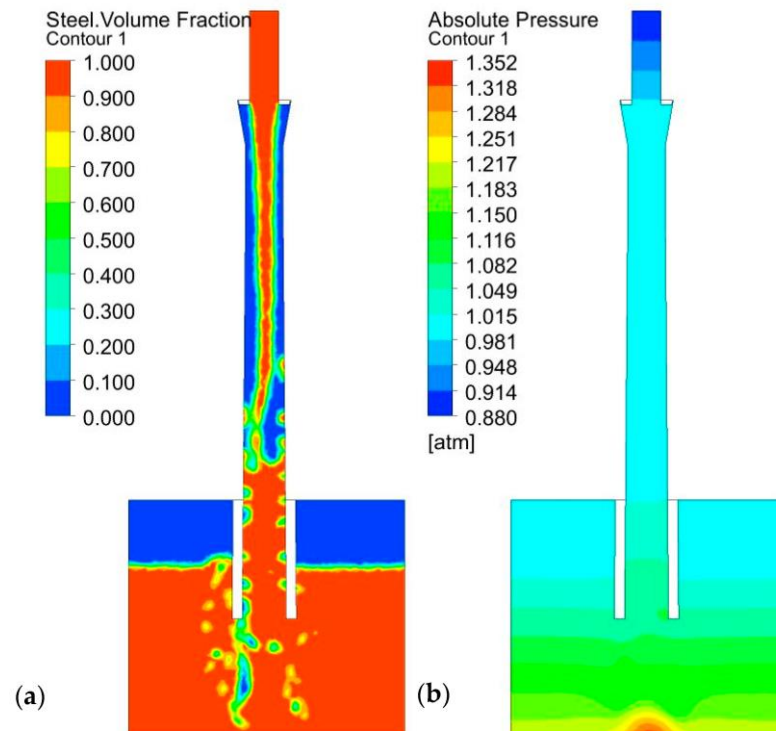


Figure 16. Predicted contours for (a) steel volume fraction and (b) absolute pressure at 42.154 s, after change of 1.2 mm gap boundary condition from wall to pressure outlet on the symmetry plane.

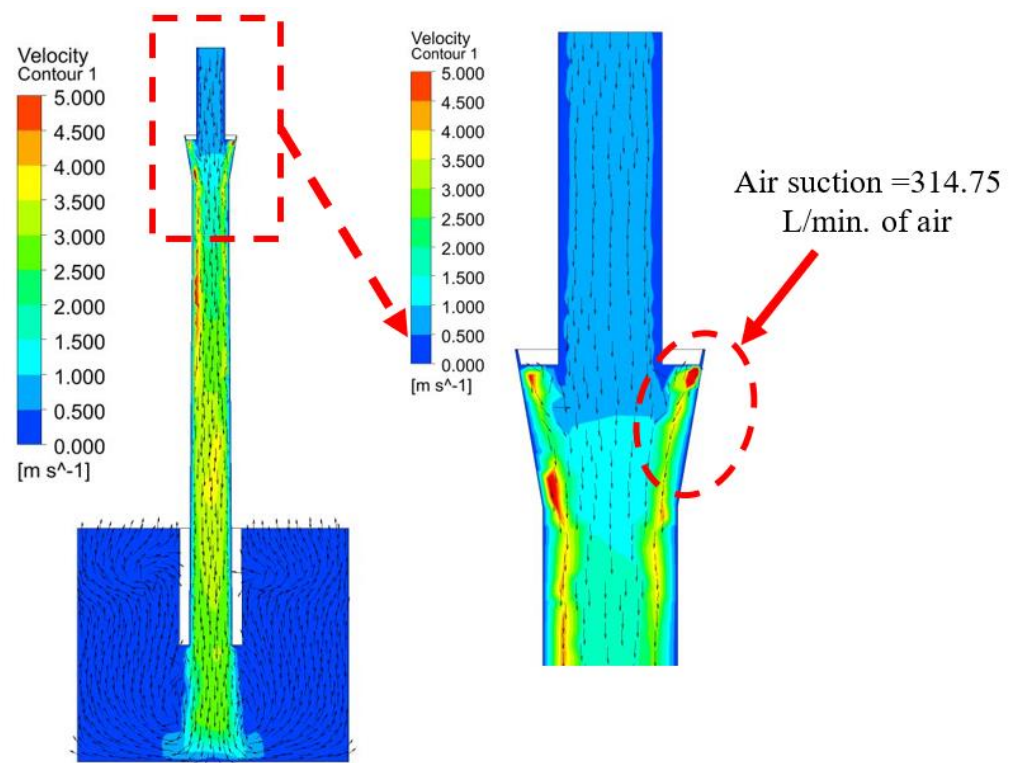


Figure 17. Predicted velocity contour with vectors and detail at the lower nozzle–Ladle Shroud joint at 42.154 s on the symmetry plane.

With the construction of the full-scale water model, Ladle Shroud, and tundish tank, an initial experiment was performed during the start-up and filling stage to qualitatively assess the multi-phase flow within the system. The results shown in Figure 18 confirm the mathematical model's predictions. It can be said, based on the comparison of the mathematical results and the water model experiments shown in Figure 18, that when a 1.2 mm gap occurs, this will allow for air infiltration at the nozzle–Ladle Shroud joint, causing a multi-phase flow system to develop within either a diverging or a reverse-tapered Ladle Shroud. This involves the following sequence of events: the incoming liquid fills the lower nozzle with liquid; then, the falling turbulent liquid stream forms in the lower nozzle–Ladle Shroud connection/joint to form a multi-phase turbulent flow within the Ladle Shroud, which subsequently exits. The exiting gas then forms gas bubbles, which rise through the liquid surface in the tundish. The previous summary is valid for both a non-gas shrouded system and a gas shrouded system. For both systems, an uncontrolled multi-phase flow regime will normally be present during the filling stage, forming air bubbles of different, uncontrolled sizes. These will promote the reoxidation of the liquid steel, thereby forming oxide inclusions and contaminating the liquid steel in a tundish. For a gas shrouded system, after the filling stage, argon bubbles of various sizes will again exit through the surface and perturb the overlaying slag, promoting the formation of oxidizing slag inclusions, unless the amounts and pressure of argon are closely controlled. This is not generally the case within the global steel industry.

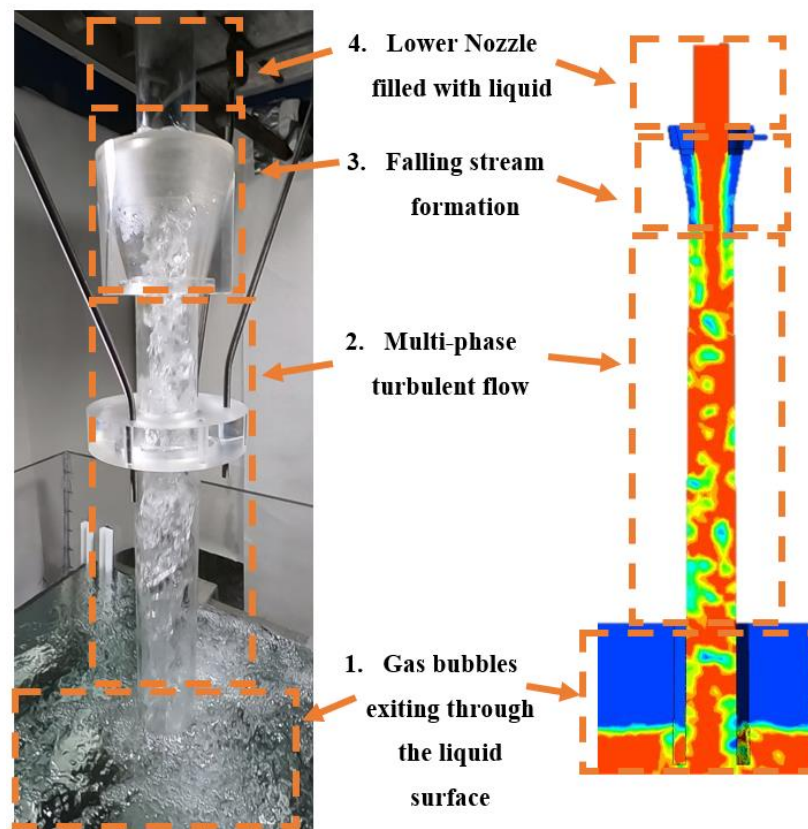


Figure 18. Multi-phase flow development inside a diverging ID Ladle Shroud in physical and mathematical modelling.

4. Conclusions

- A novel transient flow visualization of the filling stage of a tapered Ladle Shroud was mathematically modeled. This enables one to create a multi-phase flow visualization of the transient phenomena occurring within the Ladle Shroud–tundish system, from the start of pouring steel into a tundish until reaching steady-state conditions. This in turn allows one to predict phenomena such as steel splashing and time-dependent steel–air–argon interactions.
- Air suction through a 1.2 mm gap was simulated and quantified, revealing that it is possible to experience an instantaneous air suction flow of 314.75 L/min for the case of sudden misalignment of a perfectly placed Ladle Shroud with no air infiltration.
- In steady-state operation, the two-phase flow (steel–argon) will generate gas bubbles with a maximum size of around 20 mm diameter exiting the Ladle Shroud, which will likely perturb the slag layer, generating a Slag Open Eye (SOE), and entrain slag inclusions.
- A full-scale physical model of a tundish–Ladle Shroud system was successfully built for qualitative validation of the mathematical model and for further experimental and CFD research. The initial turbulent multi-phase flow within the Ladle Shroud predicted mathematically was thereby validated qualitatively.
- The present findings can help one to develop alternative designs to suppress the observed turbulent multi-phase flow and improve the performance of Ladle Shrouds in steelmaking operations.

Author Contributions: Conceptualization: R.I.L.G. and M.M.I.; methodology: R.I.L.G. and M.M.I.; software: D.R.G.-M. and R.I.L.G.; validation: D.R.G.-M., B.G. and C.L.; formal analysis: R.I.L.G., M.M.I. and D.R.G.-M.; resources: B.G., C.L., R.I.L.G. and M.M.I.; writing—original draft preparation: D.R.G.-M.; writing—review and editing: R.I.L.G. and M.M.I., supervision: R.I.L.G. and M.M.I. All authors have read and agreed to the published version of the manuscript.

Funding: This research was funded by the NSERC and the CQRDA. Grant number G272032.

Data Availability Statement: Data is contained within the article.

Acknowledgments: The authors acknowledge the financial support received from the Natural Sciences and Engineering Research Council of Canada (NSERC) and the Aluminum Research and Development Centre of Quebec (CQRDA), as well as member companies of the McGill Metals Processing Centre. The authors would also like to acknowledge the support in software licensing received from ANSYS Inc. (Canonsburg, PA, USA) to facilitate this research.

Conflicts of Interest: The authors declare no conflict of interest.

References

1. Wang, L.; Lee, H.-G.; Hayes, P. Modelling of air ingress and pressure distribution in ladle shroud system for continuous casting of steel. *Steel Res.* **1995**, *66*, 279–286. [\[CrossRef\]](#)
2. Singh, P.K.E.; Mazumdar, D. A Physical Model Study of Two-Phase Gas–Liquid Flows in a Ladle Shroud. *Metall. Mater. Trans. B* **2018**, *49*, 1945–1962. [\[CrossRef\]](#)
3. Singh, P.K.E.; Mazumdar, D. Mathematical Modelling of Gas–Liquid, Two-Phase Flows in a Ladle Shroud. *Metall. Mater. Trans. B* **2019**, *50*, 1091–1103. [\[CrossRef\]](#)
4. Zhang, J.; Qing, L.I.U.; Yang, S.; Jingshe, L.I.; Chen, Z.; Jiang, Z. Advances in Ladle shroud as a functional device in tundish metallurgy: A review. *ISIJ Int.* **2019**, *59*, 1167–1177. [\[CrossRef\]](#)
5. Morales-Higa, K.; Guthrie, R.I.L.; Isac, M.; Morales, R.D. Ladle Shroud as a Flow Control Device for Tundish Operations. *Metall. Mater. Trans. B* **2013**, *44*, 63–79. [\[CrossRef\]](#)
6. Zhang, J.; Yang, S.; Li, J.; Tang, H.; Jiang, Z. The Effect of a Dissipative Ladle Shroud on Mixing in Tundish: Mathematical and Experimental Modelling. *High Temp. Mater. Process.* **2018**, *37*, 25–32. [\[CrossRef\]](#)
7. Zhang, H.; Fang, Q.; Deng, S.; Liu, C.; Ni, H. Multiphase Flow in a Five-Strand Tundish Using Trumpet Ladle Shroud during Steady-State Casting and Ladle Change-Over. *Steel Res. Int.* **2019**, *90*, 1800497. [\[CrossRef\]](#)
8. Xu, R.; Ling, H.; Wang, H.; Chang, L.; Qiu, S. Investigation on the Effects of Ladle Change Operation and Tundish Cover Powder on Steel Cleanliness in a Continuous Casting Tundish. *Steel Res. Int.* **2021**, *92*, 2100072. [\[CrossRef\]](#)
9. Chatterjee, S.; Li, D.; Chattopadhyay, K. Modeling of liquid steel/slag/argon gas multiphase flow during tundish open eye formation in a two-strand Tundish. *Metall. Mater. Trans. B* **2018**, *49*, 756–766. [\[CrossRef\]](#)
10. Mukherjee, S.; Mazumdar, D. Physical and Mathematical Modeling of Argon Flow and Distribution Around a Ladle Shroud-Collector Nozzle (LS-CN) Assembly. *Metall. Mater. Trans. B* **2022**, *53*, 2600–2617. [\[CrossRef\]](#)
11. Mukherjee, S.; Mazumdar, D. A New Inert Gas Delivery Design for Improved Shielding of Ladle Shroud–Collector Nozzle (LS–CN) Assembly: Modeling, Design, and Industrial-Scale Validations. *Steel Res. Int.* **2022**, *93*, 2100843. [\[CrossRef\]](#)
12. Mukherjee, S.; Mazumdar, D. Air Ingression in Ladle Shrouds, Tundish Open Eye Formation, Their Inter-dependance and Correlations: A Physical Model Investigation. *Metall. Mater. Trans. B* **2022**, *53*, 3922–3933. [\[CrossRef\]](#)
13. *ANSYS Fluent Theory Guide*; 2600 ANSYS Drive; ANSYS Inc.: Canonsburg, PA, USA, 2021.
14. Singh, P.K.; Tiwari, R.; Mazumdar, D.; Dutta, A. Modeling of two phase, gas-liquid flows in a ladle shroud. In Proceedings of the 7th International Congress on Science and Technology of Steelmaking, Milano, Italy, 13–15 June 2018.
15. Chattopadhyay, K.; Hasan, M.; Isac, M.; Guthrie, R. Physical and Mathematical Modeling of Inert Gas-Shrouded Ladle Nozzles and Their Role on Slag Behavior and Fluid Flow Patterns in a Delta-Shaped, Four-Strand Tundish. *Metall. Mater. Trans. B* **2010**, *41*, 225–233. [\[CrossRef\]](#)

Disclaimer/Publisher’s Note: The statements, opinions and data contained in all publications are solely those of the individual author(s) and contributor(s) and not of MDPI and/or the editor(s). MDPI and/or the editor(s) disclaim responsibility for any injury to people or property resulting from any ideas, methods, instructions or products referred to in the content.